Journal of Catalysis **193,** 16–28 (2000)
doi:10.1006/jcat.2000.2883, available online at http://www.idealibrary.com on IDEAL®

Catalytic Reduction of Acetic Acid, Methyl Acetate, and Ethyl Acetate over Silica-Supported Copper

M. A. Natal Santiago, M. A. Sánchez-Castillo, R. D. Cortright, and J. A. Dumesic[1]

Department of Chemical Engineering, University of Wisconsin, Madison, Wisconsin 53706

Received June 17, 1999; revised March 30, 2000; accepted March 30, 2000

Microcalorimetric, infrared spectroscopic, and reaction kinetics measurements are combined with quantum-chemical calculations based on density-functional theory to investigate the selective reduction of acetic acid, methyl acetate, and ethyl acetate over silica-supported copper catalysts. Experimental values for initial heats of dissociative adsorption of methyl acetate, ethyl acetate, acetaldehyde, methanol, and ethanol on silica-supported copper are estimated to be 124, 130, 130, 128, and 140 kJ mol^{-1}, respectively. These values are in agreement with adsorption energies predicted from DFT calculations using Cu_{13} clusters. Experimental values of activation energies for the dissociation of acetic acid, methyl acetate, ethyl acetate, and acetaldehyde on copper are estimated to be 83, 67, 62, and 75 kJ mol^{-1}, respectively. Results from DFT calculations also indicate that the activation energy for dissociation decreases from acetic acid to methyl acetate to ethyl acetate. The rate of reduction of *n*-alkyl acetates appears to be determined by the dissociative adsorption of these molecules and by the hydrogenation of surface acyl species.

Key Words: **carboxylic; ester; hydrogenolysis; acetaldehyde; methanol; ethanol; alcohol.**

INTRODUCTION

The catalytic reduction of esters and carboxylic acids to alcohols encompasses reactions in which the C–O bond adjacent to a carbonyl group is cleaved according to the following stoichiometry,

$$R_A COOR_B + 2H_2 \rightleftharpoons R_A CH_2OH + R_B OH, \qquad [1]$$

where R_A represents an alkyl group and R_B represents another alkyl group or hydrogen. Of particular interest is the reduction of diesters and carboxylic acids to diols, which are used in the production of polyesters. For example, the catalytic reduction of diesters and carboxylic acids provides an environmentally benign alternative to existing energy-intensive processes for the production of 1,2-ethanediol (ethylene glycol), 1,2-propanediol, and 1,4-butanediol (1, 2). Alcohols are also used in the production of surfactants and additives present in detergents and lubricant fluids (3–7).

Copper-based catalysts typically exhibit high selectivity for the conversion of esters and carboxylic acids to alcohols (1). In fact, copper-based materials have been employed in the majority of applications since they were first used for the reduction of methyl formate (8). Catalysts for the reduction of esters and carboxylic acids have generally been prepared by mixing hydrogenating metals (e.g., Fe, Co, Ni, Cu, Zn) with various oxides (e.g., ZrO_2, V_2O_5, Cr_2O_3, WO_3) (9–18); however, the most widely used materials appear to be based on copper chromite (19). In addition, silica-supported copper and Raney copper have been shown to be as effective as copper chromite catalysts for the reduction of alkyl formates (17, 18, 20–22) and aliphatic esters (23–32).

Previous investigations (29) suggest that the reduction of ethyl acetate over copper-based catalysts proceeds via dissociative adsorption of the reagent into CH_3C^*O and $C_2H_5O^*$ species, where $*$ represents a surface site. Accordingly, one may suggest that the reduction of $R_A COOR_B$ molecules over copper-based catalysts proceeds via dissociative adsorption of the reagent into $R_A C^*O$ and $R_B O^*$ species, and subsequent hydrogenation of these species yields the desired alcohols. In addition, these reactions typically involve the partial hydrogenation of $R_A C^*O$ fragments to yield aldehydes as well as the reversible dehydrogenation of alcohols to form aldehydes:

$$R_A CH_2OH \rightleftharpoons R_A CHO + H_2. \qquad [2]$$

Reaction [2] is typically equilibrated during reduction of esters over silica-supported copper at temperatures near 570 K (30, 32). In addition, transesterification reactions occur over copper catalysts according to the following stoichiometry:

$$2R_A COOR_B + 2H_2 \rightleftharpoons R_A COOCH_2R_A + 2R_B OH. \qquad [3]$$

In the present paper, we present results from experimental and theoretical studies to probe the factors controlling the catalytic reduction of acetic acid, methyl acetate,

[1] To whom correspondence should be addressed.

0021-9517/00 $35.00

and ethyl acetate to the corresponding alcohols over silica-supported copper. Reaction kinetics measurements were conducted to assess the activity and stability of the catalyst over a range of temperatures and partial pressures of reactants; heat-flow microcalorimetry was used to measure energies of interaction between the catalyst surface and various gaseous molecules involved in the reduction process; Fourier-transform infrared (FTIR) spectroscopy was used to study the nature of surface species formed on the catalyst at various conditions; and quantum-chemical calculations based on density-functional theory (DFT) were performed to probe potential energy surfaces for interactions of copper with molecular species involved in the reduction scheme. We will show that the overall rates of conversion of acetic acid, methyl acetate, and ethyl acetate over metallic copper are determined by the dissociative adsorption of these probe molecules and by the hydrogenation of surface acyl species.

METHODOLOGY

Samples containing 5 wt% copper (analyzed by Galbraith Laboratories) were prepared by ion exchange onto the surface of silica (Cab-O-Sil from Cabot Corp., 380 $m^2\ g^{-1}$) using an aqueous solution of $Cu(NO_3)_2$ (Aldrich) (33). The degree of exchange was controlled by the maintaining of the pH of the slurry at ~11 for 4 h through the periodic addition of NH_4OH (Aldrich). The resulting material was filtered and dried overnight in air at 393 K. The material was subsequently calcined in flowing 20% O_2/He for 2 h at 600 K, reduced in flowing hydrogen for 12 h at 600 K, and stored for later use. Approximately 19 ± 2% of the total number of copper atoms were metallic surface atoms, as determined by N_2O decomposition on copper at 370 K (34–39). It was assumed in this analysis that each oxygen atom deposited on the catalyst by N_2O corresponds to two metallic surface atoms. Copper atoms are likely distributed between bulk metallic clusters and oxide patches associated with the silica support. Given that the reduction of esters and carboxylic acids is believed to occur primarily on metallic copper (1), the presence of copper oxides is not expected to significantly affect our catalytic measurements.

Reaction kinetics studies were conducted using a stainless-steel apparatus and a Pyrex, downflow reactor operating at atmospheric pressure. Studies of the reduction of acetic acid, methyl acetate, and ethyl acetate (Aldrich) were conducted using approximately 1 g of 5% Cu/silica (35–80 mesh) at 570 K, with total gas flow rates from 25 to 200 STP $cm^3\ min^{-1}$ (sccm) and varying molar ratios of hydrogen to acid or ester. Measurements were made at temperatures from 500 to 580 K. The feed to the reactor consisted of hydrogen (Liquid Carbonic) and the reactant acid or ester molecule of interest, except when determining orders of reaction, in which case helium (Liquid Carbonic) was used as a diluent. Helium was purified by flowing through OxyTrap (Alltech) followed by a bed of activated molecular sieves (Davison, 13X) at 77 K. Hydrogen was purified by flowing through a DeOxo unit (Engelhard) followed by a bed of activated molecular sieves at 77 K.

The reactant acid or ester molecules were fed to the reactor by flowing hydrogen or helium through an evaporator containing the corresponding liquid, normally at 290 K. The gases leaving the reactor were sampled using an eight-port valve with matching sample loops. The products formed during studies of methyl acetate and ethyl acetate reduction were analyzed using a gas chromatograph equipped with a thermal-conductivity detector at 373 K and a packed column at 398 K (Alltech; 5% carbowax 20M on 80–120 mesh carbograph 1AW; stainless-steel, length = 3 m, i.d. = 2.16 mm, o.d. = 3.18 mm). The gas chromatograph used for studies of acetic acid reduction was equipped with a flame ionization detector and a capillary column (19091-133 HP-INNOWax; length = 30 m, i.d. = 0.25 mm, film thickness = 0.25 μm).

Microcalorimetric measurements were performed using a Tian-Calvet, heat-flow microcalorimeter (Seteram C80) connected to a calibrated dosing system equipped with a capacitance manometer (Baratron, MKS). A detailed description of the apparatus and techniques can be found elsewhere (40, 41). Prior to each experiment, approximately 1 g of sample was outgassed in vacuum (~1 mPa) for 1 h at 400 K and for 1 h at 600 K, cooled to room temperature, reduced overnight in 100 kPa of hydrogen at 600 K, outgassed in vacuum for 2 h at 600 K, and cooled to room temperature. The microcalorimetric cells were then placed in the isothermal block, and measurements were initiated after the cells had equilibrated with the microcalorimeter at 300 K.

Infrared absorption spectra were collected at room temperature using a FTIR spectrometer (Mattson Galaxy 5020) with a resolution of 2 cm^{-1}. Samples of 5% Cu/silica (10–30 mg) were pressed into self-supporting wafers (12 mm in diameter) at a pressure of approximately 60 MPa. Prior to measurements, samples were outgassed in vacuum for 2 h, calcined in flowing 20% O_2/He for 2 h, reduced in flowing hydrogen for 12 h, and subsequently outgassed in vacuum for 2 h. All treatments were conducted at 600 K inside a cell equipped with CaF_2 windows. Spectra were collected before and after the samples were exposed to specific pressures of the probe molecules, and these spectra were subtracted to generate difference spectra. To investigate the reversibility of adsorption processes, spectra were collected after the sample was outgassed overnight at room temperature and after it was outgassed for 2 h at 600 K.

Quantum-chemical calculations were performed on the basis of DFT using the three-parameter functional B3LYP (42) along with Gaussian-type basis sets (43). It should be noted that DFT functionals are known to work well

for the prediction of thermochemical properties of systems containing light atoms, but they become less useful for the description of heavy atoms or highly charged systems (44).

The chemical behavior of supported copper was simulated using a cluster containing 13 metal atoms resembling an icosahedron. All surface atoms in this Cu_{13} cluster have the same coordination number of 6, thereby eliminating the existence of edge and corner atoms with lower coordination numbers. It should be noted that quantum-chemical calculations within the cluster approximation are dependent on the number of surface and bulk atoms incorporated into the model; therefore, results from these calculations should only be used to deduce trends in bonding and reactivity for various species adsorbed on copper.

DFT calculations were conducted using the basis set 6-31G** for carbon and hydrogen atoms, 6-31+G** for oxygen atoms, and Los Alamos effective core potential (LanL2) (45–47) for copper atoms. Detailed information about the methods used can be found elsewhere (48, 49). The calculations were performed using the software package Jaguar (50) on DEC Alpha computers. Structural parameters were determined by optimization to stationary points on the corresponding potential energy surface (PES) using Cartesian coordinates. Energetic predictions were not corrected by changes in zero-point energies.

Mulliken population analyses were used to examine trends in the relative strengths of C–O bonds adjacent to the carbonyl groups in acetic acid, methyl acetate, and ethyl acetate. However, we note that Mulliken charges are only useful qualitatively because they are based on a simple scheme to assign electronic charges to atoms in molecules.

Transition states were located on the corresponding PES to estimate activation energies for various reactions on copper. The location of transition states employed a STQN method, which uses a linear or quadratic synchronous transit approach to reach the quadratic region of the PES, followed by a quasi-Newton or eigenvalue-following algorithm to complete the optimization (51). The clusters resulting from optimizations were classified as local minima or transition states on the PES by calculation of the Hessian matrix. For local minima, the eigenvalues of the Hessian matrix were all positive, whereas for transition states only one eigenvalue was negative (43). Cartesian coordinates of the clusters in this report can be found elsewhere (52). Typically, the error associated with the use of DFT methods for the estimation of reaction energetics is between 20 and 40 kJ mol^{-1} (48, 49), depending on the energy functional, basis sets, and size of the molecular cluster used.

RESULTS

Reaction Kinetics

In general, we found that silica-supported copper displays stable catalytic activity for the reduction of acetic acid, methyl acetate, and ethyl acetate for extended periods of time (e.g., 10 h), and the catalyst can be regenerated after prolonged use by standard calcination and reduction procedures. Steady-state activity was normally achieved after 1 h on stream. A blank experiment showed that silica does not catalyze the conversion of the esters or acetic acid under our reaction conditions.

Rates of reduction versus temperature and molar hydrogen-to-ester (or acid) ratios are plotted in Figs. 1a and 1b. These rates are expressed as turnover frequencies, calculated by normalizing the rate of reaction by the number of surface metallic copper atoms ($\sim$160 μmol g^{-1}) determined from N_2O decomposition. The partial pressures of acetic acid, methyl acetate, and ethyl acetate used for these studies were 1, 3, and 4 kPa, respectively. Acetic acid is converted to water, ethanol, acetaldehyde, ethyl acetate, and less than 5 ppm of hydrocarbons. Methyl acetate is converted to methanol, ethanol, acetaldehyde, and ethyl acetate. Ethyl acetate is converted to acetaldehyde and ethanol. In all cases, the amount of acetaldehyde produced is equilibrated with hydrogen and ethanol, according to reaction [2].

Kinetic orders of reaction with respect to the partial pressures of hydrogen and esters were determined at 570 K, as shown in Figs. 1c and 1d. Kinetic orders with respect to hydrogen are equal to 0.33, 0.55, and 0.61 for the conversion of acetic acid, methyl acetate, and ethyl acetate, respectively, in agreement with previous reports (30). The partial pressures of acetic acid, methyl acetate, and ethyl acetate used in these studies were 1, 3, and 4 kPa, respectively.

Kinetic orders with respect to methyl acetate and ethyl acetate are also fractional (e.g., near 0.5). In addition, these kinetic orders generally decrease with increasing ester pressures. The partial pressure of hydrogen used for these studies was 70 kPa. It was found in a separate experiment that only traces of acetaldehyde and ethanol are produced when ethyl acetate is flowed in helium over the catalyst at 570 K in the absence of hydrogen.

Microcalorimetry and FTIR

Microcalorimetric data for the adsorption of methyl acetate, ethyl acetate, acetaldehyde, methanol, and ethanol on silica-supported copper at 300 K are shown in Fig. 2. These data are plotted as differential heats of adsorption versus surface coverage. For convenience, differential heats of adsorption have been defined as absolute values of changes in enthalpy associated with adsorption processes. Surface coverages have been normalized by the number of metallic surface copper atoms (160 μmol g^{-1}).

In a separate study, we have reported on the adsorption of alcohols (53) and carbonyl-containing organic molecules (54) on silica. These molecules adsorb through the formation of multiple (i.e., two or three) hydrogen bonds with

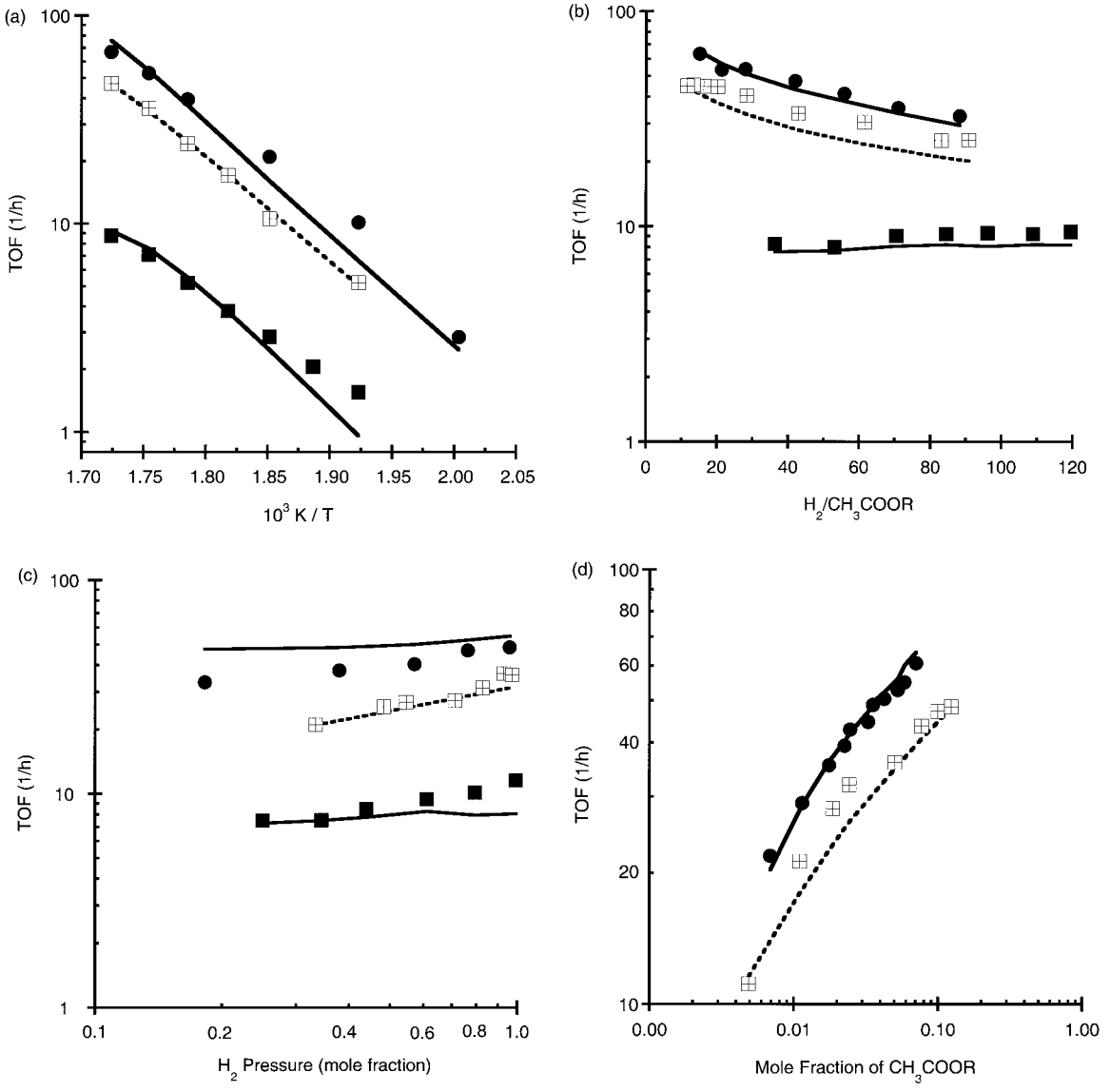

FIG. 1. Turnover frequencies for conversion of acetic acid (■), methyl acetate (⊞), and ethyl acetate (●) over 5% Cu/silica as a function of (a) temperature, (b) molar H_2-to-probe-molecule ratio, (c) inlet concentration of hydrogen, and (d) inlet concentration of ester. Solid curves correspond to predictions based on the kinetic models in Table 3.

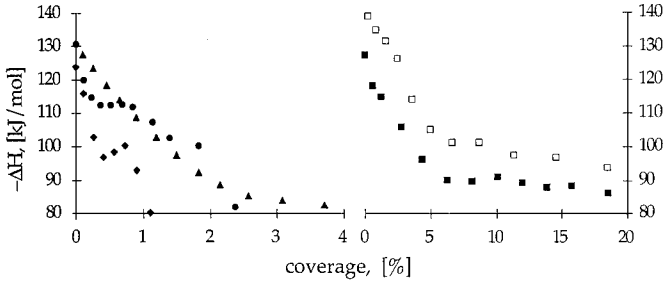

FIG. 2. Differential heats versus adsorbate coverage (as a fraction of the copper surface sites) for adsorption of methanol (■), ethanol (□), acetaldehyde (▲), methyl acetate (◆), and ethyl acetate (●) on 5% Cu/silica at 300 K.

hydroxyl groups on the silica surface. The average energy of each hydrogen bond is approximately 30 kJ mol^{-1}. These hydrogen-bonded species do not react further with silica pretreated as described in this report, and they can be removed from silica by evacuation at temperatures below 575 K.

Initial heats for the adsorption of methyl acetate, ethyl acetate, acetaldehyde, methanol, and ethanol on silica-supported copper are 124, 130, 130, 128, and 140 kJ mol^{-1}, respectively. Differential heats of adsorption decrease with increasing coverage. At coverages higher than 2%, the differential heats decrease below 90 kJ mol^{-1}, and it is not possible to differentiate between the adsorption of the probe

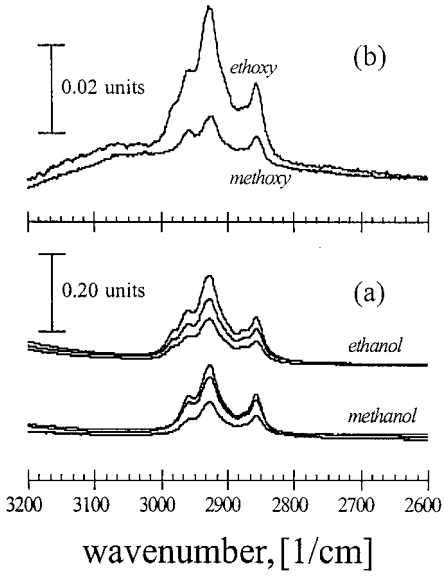

FIG. 3. FTIR spectra for methanol and ethanol on 5% Cu/silica (a) at room temperature and (b) after evacuation at 600 K.

molecules on copper and adsorption on silica. Specifically, a heat of adsorption equal to 90 kJ mol^{-1} corresponds to a desorption rate coefficient of the order of 1 h^{-1}, thus leading to nonequilibrated adsorption for the time constants of our microcalorimetric measurements. Therefore, this situation corresponds to limited mobility of the probe molecules on silica-supported copper at 300 K. Accordingly, as the coverage increases, adsorption sites are not titrated in order of decreasing strength, and the microcalorimetric data represent an average of heats of adsorption on the metal and the support. For this reason, initial heats of adsorption represent a lower limit of the heat of adsorption of the probe molecules on copper. Our attempts to facilitate equilibration of adsorbates with the catalyst sample by increasing the adsorption temperature to 400 K caused decomposition of these species, yielding gaseous products such as hydrogen, aldehydes, and carbon monoxide.

Infrared absorption spectra for methanol and ethanol on silica-supported copper are shown in Fig. 3a. These difference spectra were collected after adsorption of the alcohols at room temperature on copper for surface coverages ranging from 2% to 12%. The observed C–H stretching vibrations are listed in Table 1. Bands associated with O–H stretching (3400–4000 cm^{-1}) and C–H bending (1300–1500 cm^{-1}) were also observed; however, the intensities of these bands were much lower than those of the bands shown in Fig. 3a. When molecularly adsorbed alcohols are removed from the surface by evacuation at 600 K, it can be seen in Fig. 3b that residual surface species are still present. Since alcohols can be removed completely from silica by this evacuation procedure (53), we suggest that these residual species are adsorbed on copper.

TABLE 1

Vibrational bands (cm^{-1}) of Methoxy and Ethoxy Species on 5% Cu/Silica (Fig. 3b)

	Methoxy		Ethoxy	
	Measured	DFT	Measured	DFT
$\nu''_{as}(CH_3)$	(2960)	(2948)	(2982)	2988
$\nu'_{as}(CH_3)$	(2960)	(2948)	(2982)	2986
$\nu''(CH_2)$	—	—	2958	2943
$2\delta''_{as}(CH_3)$	2926	2897	—	—
$\nu_s(CH_3)$	2858	2879	2929	2908
$\nu'(CH_2)$	—	—	2858	2897

Note. DFT predictions correspond to species in Figs. 4 and 5, and they have been scaled by a factor of 0.96. The bands in parentheses are either degenerate or cannot be resolved.

DFT Calculations

The average length and energy of Cu–Cu bonds in the optimized 13-atom copper cluster were 260 ± 10 pm and 165 kJ mol^{-1}. These values compare well with the length of 256 pm and energy of 195 kJ mol^{-1} typically associated with these bonds in bulk metallic copper.

The optimized structure of methoxy species on Cu_{13} is shown in Fig. 4. These species can form via dissociative

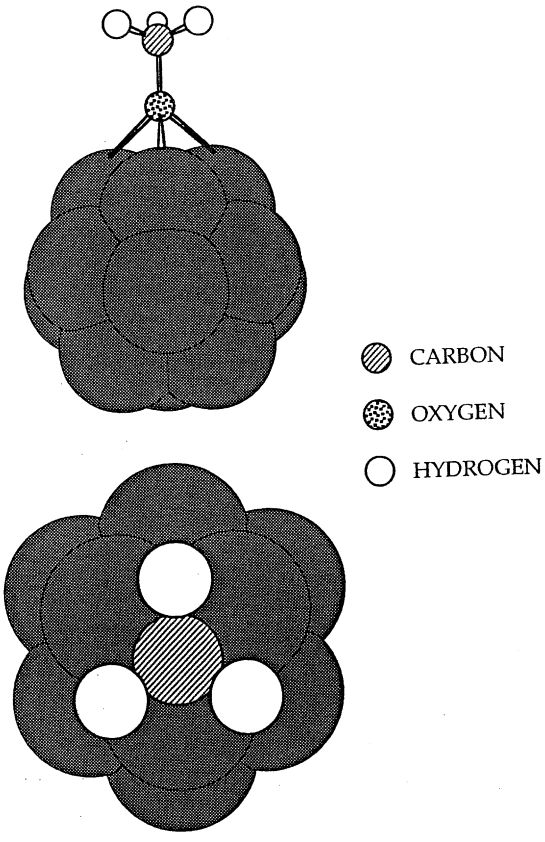

FIG. 4. Front and top views of the optimized structure of methoxy species on a Cu_{13} cluster.

TABLE 2

DFT Predictions of Energetics (kJ mol^{-1}) of Various Reactions

	$-\Delta E$ (DFT)	$-\Delta H$ (Exp)
$H_2 + 2^* \rightarrow 2H^*$	—	90
$MeOH + ^* \rightarrow CH_3O^* + \frac{1}{2}H_2$	130	83
$EtOH + ^* \rightarrow C_2H_5O^* + \frac{1}{2}H_2$	132	95
$AcH + ^* \rightarrow CH_3C^*O + \frac{1}{2}H_2$	59	85
$MA + 2^* \rightarrow CH_3C^*O + CH_3O^*$	166	124
$EA + 2^* \rightarrow CH_3C^*O + C_2H_5O^*$	168	130

Note. Experimental values are derived from initial heats of adsorption in Fig. 2 and they represent the lower limit for adsorption of the probes molecules on copper.

adsorption of methanol or methyl acetate. The cluster was constrained to have C_s symmetry during optimization. Methoxy species are predicted to occupy a three-fold hollow site and orient with the C–O bond perpendicular to the metal surface, exhibiting C_{3v} symmetry. The energy of formation is predicted to be 130 kJ mol^{-1} relative to the reaction $CH_3OH + ^* \rightarrow CH_3O^* + \frac{1}{2}H_2$, as listed in Table 2. Rotation of the methyl group to an eclipsed position relative to the hollow site increases the energy of the cluster by less than 10 kJ mol^{-1}. The lengths of C–O, C–H, and O–Cu bonds are predicted to be 143, 110, and 207 pm, respectively. The HCH, HCO, COCu, and CuOCu angles are predicted to be 108.4°, 110.5°, 127.6°, and 86.6°, respectively. Upon interaction with methoxy species, copper atoms bonded to the oxygen atom relax such that Cu–Cu bond lengths increase to 284 pm. A local frequency analysis in which only atoms in the adsorbate are displaced results in the C–H stretching bands listed in Table 1. The predicted vibrational bands are in agreement with those observed in Fig. 3b, within the typical error of 50 cm^{-1} associated with quantum-chemical calculations.

The optimized structure of ethoxy species on Cu_{13} is shown in Fig. 5. These species can form via dissociative adsorption of ethanol or ethyl acetate. The cluster was constrained to have C_s symmetry during optimization. Ethoxy species are predicted to occupy a hollow site on the metal surface. The energy of formation is predicted to be 132 kJ mol^{-1}, relative to the reaction $C_2H_5OH + ^* \rightarrow C_2H_5O^* + \frac{1}{2}H_2$ (Table 2). The lengths of C–O, C–H, and O–Cu bonds are predicted to be 144, 110, and 206 pm, respectively. The CCO angle is predicted to be 110.2°. The COCu and CuOCu angles on each side of the mirror plane are predicted to be 130.5° and 83.8°, respectively. The remaining COCu and CuOCu angles are predicted to be 123.4° and 88.8°. Consequently, the C–O bond of ethoxy species is predicted to be tilted away form the surface normal by ~10°, most likely because of interactions between copper and the alkyl chain. A local frequency analysis in which only atoms in the adsorbate are displaced results in the C–H stretching bands listed in Table 1. The predicted vibrational bands are in agreement with those observed in Fig. 3b, within the 50-cm^{-1} error of our calculations.

The optimized structure of acyl species on Cu_{13} is shown in Fig. 6. These species can form via dissociative adsorption of acetaldehyde, methyl acetate, or ethyl acetate. In this case, the cluster was not constrained during optimization. Acyl species are predicted to occupy a bridge site and orient with the C=O bond parallel to the metal surface. Predicted energies of formation with respect to various possible reactions are listed in Table 2. The lengths of C=O, C–H, C–Cu, and O–Cu bonds are predicted to be 125, 110, 198, and 208 pm, respectively. The CCCu, OCCu, CuOC, and OCC angles are predicted to be 124.8°, 117.6°, 109.6°, and 117.3°, respectively. Consequently, the CCO plane of the adsorbate is predicted to be tilted away from the surface normal by ~20°. A local frequency analysis in which only atoms in the adsorbate are displaced predicts a C=O stretching band at 1577 cm^{-1}, whereas the experimental value is 1647 cm^{-1} (29). This discrepancy may be related to the comparison in

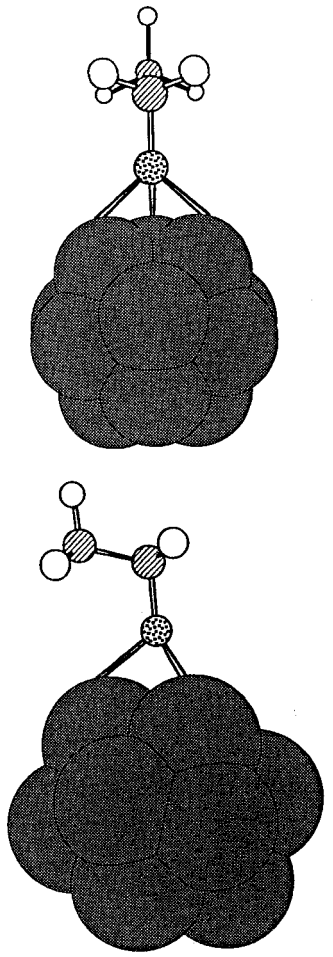

FIG. 5. Front and side views of the optimized structure of ethoxy species on a Cu_{13} cluster.

Table 2 which shows that our DFT calculations appear to overpredict the bonding energetics on copper.

Alkoxy species can undergo dehydrogenation on copper at temperatures higher than 320 K to produce an aldehyde and hydrogen (55–65). A schematic representation of the transition states for the dehydrogenation of methoxy and ethoxy species on copper and the corresponding activation energies are included in Fig. 7. The products of these transformations consist of atomic hydrogen on a three-fold hollow site plus an aldehyde molecule on a bridge site. Activation energies for the dehydrogenation of methoxy and ethoxy species are predicted to be 165 and 156 kJ mol^{-1}, respectively (see Fig. 7). These barriers are higher than the experimental ranges of 90–140 and 80–120 kJ mol^{-1} reported elsewhere (55–65). The C–O bond in these transition states is tilted toward the metal surface at an angle of about 30°, while the C–H bond being cleaved is lengthened to 184–205 pm. The imaginary mode of vibration (reaction coordinate) involves stretching of this C–H bond coupled with rocking of the alkoxy group.

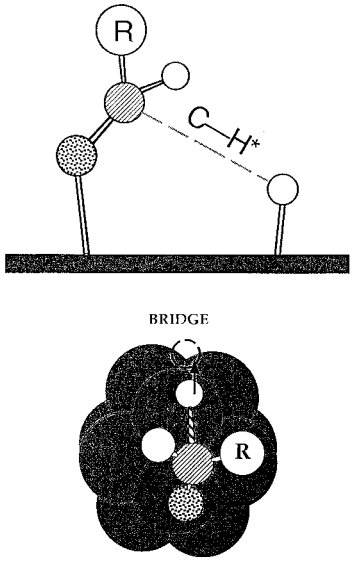

	E_a, [kJ/mol]
CH_3O^*	165
$C_2H_5O^*$	156

FIG. 7. Transition states and activation energies for dehydrogenation of methoxy and ethoxy species on copper.

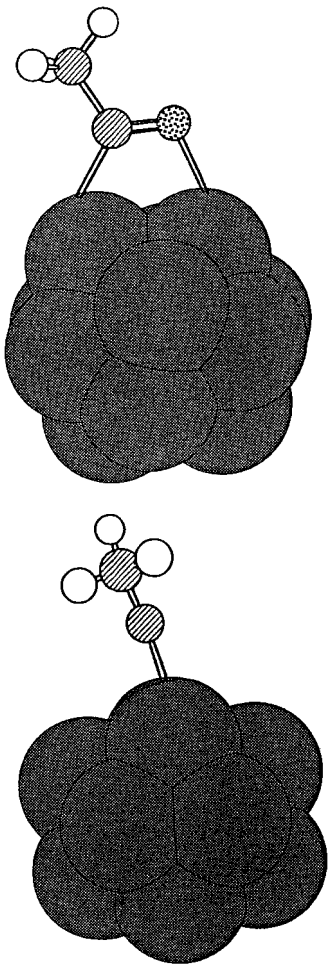

FIG. 6. Side and back views of the optimized structure of an acyl species on a Cu_{13} cluster.

Acetaldehyde, acetic acid, methyl acetate, and ethyl acetate can dissociate upon adsorption on copper through cleavage of the C–*X* bond adjacent to the carbonyl group, where *X* represents a hydroxyl group, an alkoxy group, or a hydrogen atom. A schematic representation of the transition states and the corresponding activation energies are included in Fig. 8. Activation energies are reported as a range of values because we were not able to locate rigorously first-order saddle points on the corresponding potential energy surfaces. Optimizations were complicated by loose modes of vibration involving copper atoms or the alkoxy part of the molecules. Nevertheless, our calculations suggest that the activation energy for dissociative adsorption decreases as we move from acetic acid to methyl acetate to ethyl acetate to acetaldehyde. The reaction coordinate consists of elongation of the C–*X* bond (to 178–184 pm for the *n*-alkyl acetates) coupled with a slight elongation of the C=O bond from approximately 121 pm in the gaseous molecule to about 124 pm in the adsorbed acyl group. The product of this transformation consists of an acyl group on a bridge site and a hydroxyl group, an alkoxy group, or a hydrogen atom on a nearby hollow site.

DISCUSSION

The adsorption of alcohols, mainly methanol and ethanol (55–90), on copper surfaces has been studied extensively in the literature. It has been established that, at temperatures

between 180 and 300 K, molecularly adsorbed alcohols react with the metal surface via cleavage of the O–H bond to produce alkoxy species and surface hydrogen. Our high initial heats of adsorption and FTIR investigations suggest that methanol and ethanol adsorb dissociatively on silica-supported copper at 300 K to produce methoxy and ethoxy species. Our DFT calculations suggest that methoxy species are oriented with the C–O bond perpendicular to the copper surface and exhibit local C_{3v} symmetry, whereas ethoxy species are oriented such that the C–O bond is tilted from the surface normal by $\sim 10^\circ$ and exhibit C_s symmetry. The heats of formation of methoxy and ethoxy species (from the corresponding alcohols with liberation of gaseous hydrogen) are suggested to be near 130 kJ mol^{-1} (see Table 2).

Alkoxy species can undergo dehydrogenation on copper at temperatures higher than 320 K to produce an aldehyde and hydrogen (55–65). Activation energies for the dehydrogenation of methoxy and ethoxy species on copper have been reported to be within the ranges of 90–140 and 80–120 kJ mol^{-1}, respectively, and the results from our DFT calculations predict these activation energies to be about 160 kJ mol^{-1}. Experimental investigations have also demonstrated that the activation energy for alkoxy dehydrogenation depends on the nature of the copper surface being considered. In general, it has been found that ethoxy species typically exhibit faster dehydrogenation than methoxy species under the same experimental conditions. Moreover, while methoxy species on copper typically recombine with surface hydrogen to desorb as methanol, ethoxy species tend to undergo further dehydrogenation to yield acetaldehyde (55, 56, 58, 59, 61, 64, 67).

The adsorption of ethyl acetate on copper under reduction conditions is believed to proceed via cleavage of the C–O bond adjacent to the carbonyl group (29). We extend this finding to propose that the adsorption of aliphatic esters and carboxylic acids also proceeds via cleavage of the C–O bond adjacent to the carbonyl group. Products of this reaction consist of adsorbed $R_A C^* O$ and $R_B O^*$ species. The existence of the former species on silica-supported copper has already been established (29). The IR band corresponding to C=O stretching has been assigned at 1647 cm^{-1}. The high initial heats observed from our microcalorimetric studies of methyl acetate, ethyl acetate, and acetaldehyde adsorption on silica-supported copper at 300 K as well as the observed production of gaseous species upon ester adsorption at higher temperatures provide evidence that these probe molecules adsorb dissociatively on copper.

To the best of our knowledge, there are no reports regarding the relative rates of dissociation of esters versus carboxylic acids on copper surfaces. Our DFT calculations suggest that the activation energy for dissociative adsorption increases as we move from ethyl acetate to methyl acetate to acetic acid (Fig. 8). Moreover, the rate of dissociation of these three molecules on copper is limited by cleavage of the C–O bond adjacent to the carbonyl group,

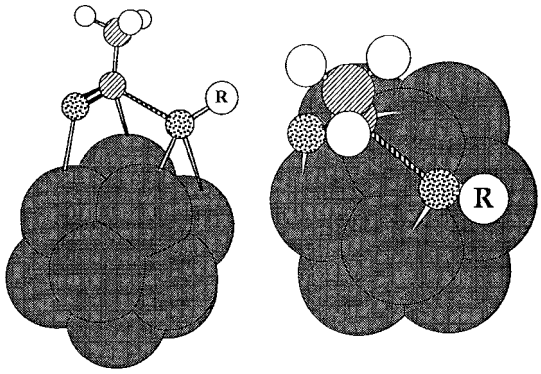

	E_a, [kJ/mol]
CH_3COOH	90–100
CH_3COOCH_3	70–80
$CH_3COOC_2H_5$	50–60
CH_3CHO	40–50

FIG. 8. Transition states and activation energies for dissociative adsorption of various carbonyl-containing organic molecules on copper.

which is affected by the ability of the *R* group in Fig. 8 to donate electronic density to the alkoxy oxygen atom. Mulliken charges associated with the acyl group in acetic acid, methyl acetate, and ethyl acetate are $+0.159e$, $+0.124e$, and $+0.122e$, respectively. These values establish a difference between the carboxylic acid and the esters. As the *R* group in Fig. 8 goes from H (acetic acid) to CH_3 (methyl acetate) to C_2H_5 (ethyl acetate), it becomes easier to cleave the C–O bond adjacent to the carbonyl group and the activation energy for dissociation decreases.

In our analyses of reaction kinetic data, we have assumed that the catalytic reductions of acetic acid, methyl acetate, and ethyl acetate proceed through the scheme described by steps 1–10 in Table 3. This reaction scheme consists of dissociative adsorption of reactants and products and surface hydrogenation reactions. To test the feasibility of this reaction scheme to describe the reaction kinetics data, it is necessary to quantify thermodynamic and kinetic parameters associated with each step. The equilibrium constants describing the formation of stable surface species are expressed in terms of the appropriate standard entropy changes and enthalpy changes. Values for standard entropies and enthalpies for the gas-phase species were obtained from the data supplied by Yaws (91). The standard state pressure is 1 atm.

We first consider the thermodynamic parameters of the reaction scheme. Surface hydrogen atoms were assumed to be immobile on the surface. The surface entropies of oxygenated species were linked together, assuming that these species exhibit similar mobility on the surface. Accordingly, the thermodynamic parameter for the surface entropies of oxygenated species is a factor that multiplied the local

TABLE 3

Parameters of the Kinetic Model Used To Describe the Reduction of Ethyl Acetate, Methyl Acetate, and Acetic Acid Over Cu/Silica

Step		ΔS^a (J/(mol K))	ΔH (kJ/mol)	E_{for} (kJ/mol)	E_{rev} (kJ/mol)
1	$EA + 2^* \rightleftharpoons CH_3C^*O + C_2H_5O^*$	−151	−86[d]	62 ± 1	148
2	$CH_3C^*O + H^* \rightleftharpoons AcH + 2^*$	171	63 ± 15	139	75 ± 1
3	$AcH + H^* \leftrightharpoons C_2H_5O^*$	−144	−131[d]	0[c]	131
4	$C_2H_5O^* + H^* \leftrightharpoons EtOH + 2^*$	172	113 ± 15	113	0[c]
5	$H_2 + 2^* \leftrightharpoons 2H^*$	−149[b]	−54 ± 30	30[b]	84
6	$MA + 2^* \rightleftharpoons CH_3C^*O + CH_3O^*$	−147	−86[d]	67 ± 1	153
7	$CH_3O^* + H^* \leftrightharpoons MeOH + 2^*$	166	113 ± 15	113	0[c]
8	$AcOH + 2^* \rightleftharpoons CH_3C^*O + HO^*$	−145	−84[d]	83 ± 2	167
9	$HO^* + H^* \leftrightharpoons H_2O + 2^*$	159	98 ± 3	98	0[c]
10	$AcOH + 2^* \leftrightharpoons CH_3C^*OO^* + \frac{1}{2}H_2$	−101	−70[e]		

Note. Adjustable parameters provide 95% confidence limits. A sticking coefficient of 1.0 was assumed for all adsorption steps.

[a] Fitted parameter is the ratio of surface entropy to the entropy for an immobile adsorbed species (S_{loc}). The value of this parameter was found to be 0.985 ± 0.025 for both the methyl acetate and ethyl acetate cases and 0.935 ± 0.022 for the acetic acid case.

[b] Surface atomic hydrogen assumed to be immobile and hydrogen adsorption step assumed activated with an activation energy of 30 kJ/mol.

[c] Nonactivated adsorption assumed for these steps.

[d] Changes in enthalpy set to maintain thermodynamic consistency for gas-phase reactions.

[e] Change in enthalpy not sensitive.

surface entropies of these species, where the local entropy, S_{loc}, for a species is defined as the vibrational and rotational entropy associated with the species. The enthalpy changes for the adsorption of acetaldehyde (step 2), ethanol (step 4), hydrogen (step 5), methanol (step 7), water (step 9), and acetic acid to form adsorbed acetate (step 10) were adjusted in the kinetic analysis. The enthalpy changes for the dissociative adsorption of ethyl acetate (step 1), methyl acetate (step 6), acetic acid (step 8), and the adsorption of acetaldehyde to form ethoxy species (step 3) were constrained to maintain thermodynamic consistency for the appropriate overall gas-phase reactions.

In the kinetic analysis, it was assumed that the adsorption steps occur with a sticking coefficient of 1.0. The activation energies for the dissociative adsorption of ethyl acetate, acetaldehyde, methyl acetate, and acetic acid were adjusted in the kinetic analysis. The steps involving dissociative adsorption of ethanol, methanol, and water were assumed to be nonactivated. Finally, the activation energy for adsorption of hydrogen on copper was set at a value of 30 kJ mol^{-1}, in agreement with the literature (92).

The results of DFT calculations outlined above provide initial estimates for activation energies and enthalpy changes associated with various steps of the reaction scheme. For example, the DFT results of Table 2 suggest similar values of the enthalpy changes for adsorption of methanol and ethanol, and these enthalpy changes were thus constrained to be equal in the analysis. Values for the fitted parameters were determined using Athena Visual Workbench (93). This software employs a general regression analysis of the reaction kinetics data with the reactor treated as a plug flow reactor. All values of the parameters were estimated at a reactor temperature of 570 K.

During the initial stages of kinetic analysis, we considered the reduction of ethyl acetate and methyl acetate. Optimized parameters for the kinetic model used to describe the catalytic reduction of these two esters are listed in Table 3. The solid curves in Fig. 1 represent predictions of the kinetic model at various reaction conditions. Good agreement is achieved between the predictions of the model and the experimental reaction kinetics data for the reduction of both ethyl acetate and methyl acetate. Furthermore, good agreement is observed between model predictions and experimental data for the individual rates of production of methanol, acetaldehyde, and ethyl acetate during the reduction of methyl acetate, as shown in Fig. 9.

This analysis suggests that adsorption steps for ethanol (step 4), hydrogen (step 5), methanol (step 7), and the adsorption of acetaldehyde to form ethoxy species (step 3) are quasi-equilibrated. The dissociative adsorption steps for ethyl acetate (step 1), acetaldehyde (step 2), and methyl acetate (step 6) appear to be slower steps, and these steps are reversible at most conditions investigated. Furthermore, the model predicts that the surface is highly covered (fractional coverages higher than 90%) with oxygenated species (methoxy, ethoxy, or acyl species).

The entropy values shown in Table 3 suggest that all adsorbed species are essentially immobile on the surface. As noted above, the enthalpy changes for desorption of methanol and ethanol (steps 4 and 7) were constrained to be equal. In addition, the enthalpy change for desorption of acetaldehyde (step 2) was lower than that for the two

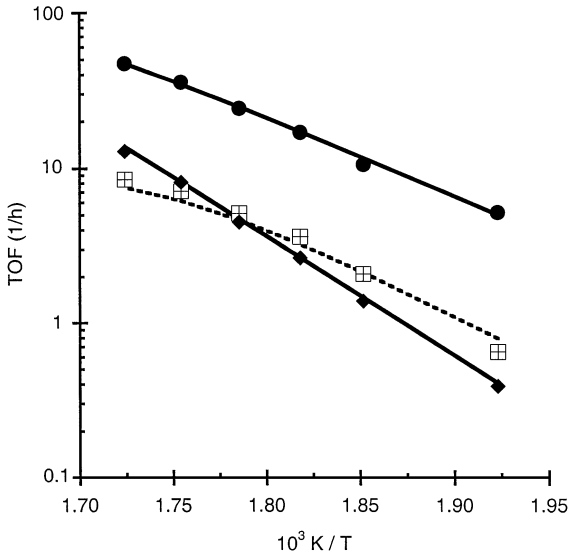

FIG. 9. Turnover frequencies for production of methanol (●), acetaldehyde (⊞), and ethyl acetate (◆) from the reduction of methyl acetate as a function of temperature. Solid curves correspond to predictions based on the kinetic model in Table 3.

alcohols. These trends are consistent with results predicted by DFT calculations shown in Table 2. While the values predicted by the DFT calculations (Table 2) are higher than those shown in Table 3, this difference may be explained by the fact that the surface is highly covered by oxygenated species whereas the DFT calculations are based on a clean surface. Furthermore, it has been suggested that DFT calculations based on clusters may predict overbinding of adsorbed species (94).

The kinetic model for the reduction of acetic acid involves the reaction steps related to the reduction of ethyl acetate (steps 1–5) plus additional steps to describe the dissociative adsorption of acetic acid on copper (step 8), the hydrogenation of hydroxyl species to water (step 9), and the equilibrated formation of acetate species on the surface (step 10). We did not include the formation of acetate species for the cases of ethyl acetate reduction or methyl acetate reduction since ethane and methane were not detected during our experiments for these cases. However, it should be easier to break the CH_3COO–H bond for acetic acid than the CH_3COO–*R* bonds in the esters, and we have, therefore, included the formation of acetate species in our kinetic model for acetic acid reduction.

Optimized values for the parameters of the kinetic model used to describe the catalytic reduction of acetic acid over silica-supported copper are listed in Table 3. Importantly, the energetic values determined from analyses of the methyl and ethyl acetate reduction data were maintained in this analysis of acetic acid reduction data. The new kinetic parameters added for acetic acid reduction were the enthalpy changes for adsorption of water and for the formation of acetate species and the activation energy for the dissociative adsorption of acetic acid. In addition, a small adjustment was made in the multiplicative factor controlling the mobilities of the adsorbed species (from 0.985 to 0.935). It can be seen in Fig. 1 that good agreement is achieved between predicted (solid curves) and experimental turnover frequencies for acetic acid conversion. Experimental and predicted rates of production of ethanol and ethyl acetate from the reduction of acetic acid are plotted in Fig. 10.

It is important to note that the kinetic model used to fit our kinetic data for the reduction of ethyl acetate, methyl acetate, and acetic acid (Table 3) suggests an important trend in the activation energies for dissociation of carbonyl-containing organic molecules; the activation energies for dissociative adsorption of acetic acid, methyl acetate, and ethyl acetate are 83, 67, and 62, respectively. These values are in general agreement with the results predicted by the DFT calculations (Fig. 8), and the activation energy barrier for dissociation of these molecules decreases as we move from acetic acid to methyl acetate to ethyl acetate.

To gain insight into the relative rates of steps in our kinetic models, we derive rate expressions in terms of De Donder relations (95–99) for the reduction of ethyl acetate (Table 3), which is the simplest reaction scheme in this study. Surface coverages can be expressed by the following relations,

$$\theta_{H^*} = \sqrt{K_5 p_{H_2} \theta_*}, \quad [4]$$

$$\theta_{EtO^*} = \frac{P_{EtOH}}{z_4 K_4 \sqrt{K_5 p_{H_2}}} \theta_*, \quad [5]$$

$$\theta_{Ac^*} = \frac{z_1 z_4 K_1 K_4 \sqrt{K_5 p_{H_2}}\, p_{EA}}{p_{EtOH}} \theta_*, \quad [6]$$

where θ^* represents the fraction of vacant sites on the

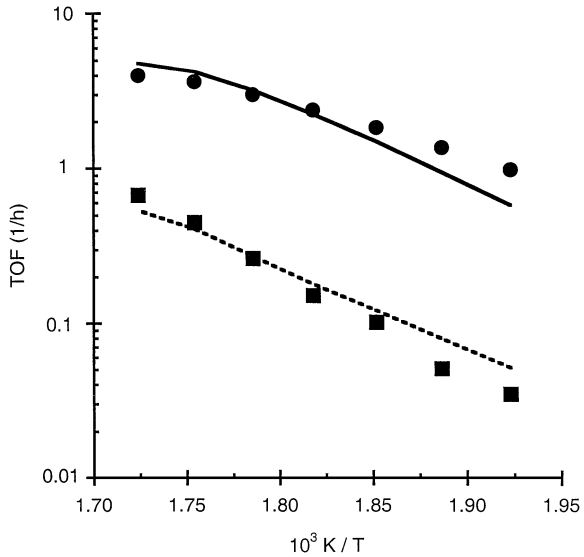

FIG. 10. Turnover frequencies for production of ethanol (●) and ethyl acetate (■) from the reduction of acetic acid as a function of temperature. Solid curves correspond to predictions based on the kinetic model in Table 3.

catalyst and the dimensionless variable z_j may be termed the reversibility of step j such that

$$z_j = \frac{\prod_i a_i^{v_{ij}}}{K_j}, \quad [7]$$

$$\prod_{j=1}^{5} z_j^{\sigma_j} = \frac{p_{\mathrm{EtOH}}^2}{K_{\mathrm{EA}}\, p_{\mathrm{EA}}\, p_{\mathrm{H_2}}^2} \equiv z_{\mathrm{t}}. \quad [8]$$

In these expressions, a_i represents the activity of species i, v_{ij} represents the stoichiometric coefficient of species i in step j, σ_j represents the stoichiometric coefficient of step j in the reaction scheme, and z_{t} represents the overall reversibility. These relations for the surface coverages can then be used to derive the following expressions for the rates of steps 1–4 in Table 3:

$$\Re_1 = k_{1\mathrm{f}} p_{\mathrm{EA}} \theta_*^2 (1 - z_1), \quad [9]$$

$$\Re_2 = \frac{k_{2\mathrm{f}} K_1 K_4 K_5 z_1 z_4 p_{\mathrm{EA}} p_{\mathrm{H_2}}}{p_{\mathrm{EtOH}}} \theta_*^2 (1 - z_2), \quad [10]$$

$$\Re_3 = k_{3\mathrm{f}} p_{\mathrm{AcH}} \sqrt{K_5 p_{\mathrm{H_2}}}\, \theta_* (1 - z_3), \quad [11]$$

$$\Re_4 = \frac{k_{4\mathrm{r}} p_{\mathrm{EtOH}}}{z_4} \theta_*^2 (1 - z_4). \quad [12]$$

Finally, the fraction of vacant sites on the catalyst is given by a site balance:

$$\theta_* = 1 - \theta_{\mathrm{Ac}^*} - \theta_{\mathrm{EtO}^*} - \theta_{\mathrm{H}^*}. \quad [13]$$

We may determine the unknown values of z_j and θ^* by solving the following steady-state relations,

$$\Re_1 = \Re_2 = \Re_3 = 1/2\Re_4, \quad [14]$$

along with the site balance.

Based on the kinetic parameters listed in Table 3, we have constructed in Fig. 11 plots of the Gibbs free energy versus reaction coordinate at partial pressures of ethyl acetate and hydrogen equal to 4 and 96 kPa and total flow rate equal to 200 sccm at 500 and 570 K. At 570 K the values of z_1, z_2, z_3, z_4, z_5, and z_{t} are equal to 0.79, 0.16, 1.00, 1.00, 1.00, and 0.12, respectively. To construct the Gibbs free energy profile, we note that, for example, the rate of step 2 can be written as follows:

$$\Re_2 = \left(\frac{k_{\mathrm{B}} T}{h}\right) \exp\left\{ \frac{\Delta^{\neq} G_2^{\circ} - RT \ln\left(K_1 K_4 K_5 z_1 z_4 \frac{a_{\mathrm{EA}} a_{\mathrm{H_2}}}{a_{\mathrm{EtOH}}}\right)}{RT} \right\} \times \theta_*^2 (1 - z_2). \quad [15]$$

Therefore, the Gibbs free energy barrier associated with step 2 under reaction conditions is given by

$$\Delta^{\neq} G_2 = \Delta^{\neq} G_2^{\circ} - RT \ln\left(K_1 K_4 K_5 z_1 z_4 \frac{a_{\mathrm{EA}} a_{\mathrm{H_2}}}{a_{\mathrm{EtOH}}}\right). \quad [16]$$

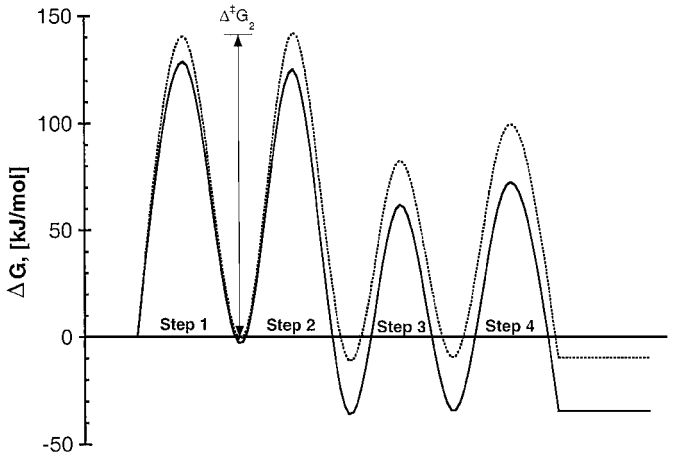

FIG. 11. Profile of Gibbs free energy versus reaction coordinate for reduction of ethyl acetate over Cu/silica at 500 K (—) and 570 K (---), partial pressures of the ester and hydrogen equal to 4 and 96 kPa, and a total flow rate equal to 200 sccm.

Since the total Gibbs free energy decreases by

$$\Delta G_1 = RT \ln(z_1). \quad [17]$$

after the occurrence of step 1, the maximum in the Gibbs free energy profile associated with step 2 is located at $\Delta G_1 + \Delta^{\neq} G_2$. Analogous analyses involving steps 1, 3, and 4 in Table 3 lead to the following expressions:

$$\Delta G_j = RT \ln(z_j), \quad [18]$$

$$\Delta^{\neq} G_1 = \Delta^{\neq} G_1^{\circ} - RT \ln(a_{\mathrm{EA}}), \quad [19]$$

$$\Delta^{\neq} G_3 = \Delta^{\neq} G_3^{\circ} - RT \ln\left(a_{\mathrm{AcH}} \sqrt{K_5 a_{\mathrm{H_2}}}\right), \quad [20]$$

$$\Delta^{\neq} G_4 = \Delta^{\neq} G_4^{\circ} - RT \ln\left(\frac{a_{\mathrm{EtOH}}}{z_4 K_4}\right). \quad [21]$$

According to our model, the reaction scheme for the reduction of ethyl acetate does not possess a rate-determining step; that is, both the dissociative adsorption of ethyl acetate (step 1) and the hydrogenation of acyl species (step 2) are critical steps in the reduction process. This conclusion is consistent with suggestions in the literature that the hydrogenation of acyl groups, formed from the dissociative adsorption of alkyl acetates, is important in controlling the overall rate of reduction of esters and carboxylic acids on copper-based catalysts, whereas the hydrogenation of alkoxy groups is rapid (29).

CONCLUSION

Experimental values of initial heats for adsorption of methyl acetate, ethyl acetate, acetaldehyde, methanol, and ethanol on silica-supported copper were estimated to be 124, 130, 130, 128, and 140 kJ mol^{-1}, respectively. These values are in accord with adsorption energetics estimated

from DFT calculations on Cu_{13} clusters. Results from kinetic analyses and DFT calculations indicate that the rate of dissociation on copper increases in the order from acetic acid to methyl acetate to ethyl acetate. The corresponding experimental values of the activation energies are estimated to be 83, 67, and 62 kJ mol^{-1}, respectively. On the basis of our kinetic analyses, we suggest that the rate of reduction of *n*-alkyl acetates is determined by the dissociative adsorption of these molecules and by the surface hydrogenation of surface acyl species.

ACKNOWLEDGMENTS

We want to thank the Office of Basic Energy Sciences of the Department of Energy as well as the National Center for Clean Industrial and Treatment Technologies for financial support. We also want to thank Josephine M. Hill for helpful discussions.

REFERENCES

1. Turek, T., Trimm, D. L., and Cant, N. W., *Catal. Rev.-Sci. Eng.* **36**(4), 645 (1994).
2. Datta, R., *in* "Kirk–Othmer Encyclopedia of Chemical Technology" (J. I. Kroschwitz and M. Howe-Grant, Eds.), 4th ed., Vol. 13, pp. 1042–1062. John Wiley & Sons, New York, 1995.
3. Studt, P., *Tribology Int.* **22**(2), 111 (1989).
4. Bowden, F. P., and Tabor, D., "The Friction and Lubrication of Solids," Part 1, Vol. 1. Oxford University Press, New York, 1950.
5. Bowden, F. P., and Tarbor, D., "The Friction and Lubrication of Solids," Part 2. Oxford University Press, New York, 1964.
6. McFadden, C. F., and Gellman, A. J., *Langmuir* **11**, 273 (1995).
7. McFadden, C. F., and Gellman, A. J., *Surf. Sci.* **409**, 171 (1998).
8. Christiansen, J. A., U.S. Patent 1,302,011, 1919.
9. Adkins, H., and Folkers, K., *J. Am. Chem. Soc.* **53**, 1095 (1931).
10. Adkins, H., *in* "Organic Reactions" (R. Adams, Ed.), Vol. 8. John Wiley & Sons, New York, 1954.
11. Folkers, K., and Adkins, H., *J. Am. Chem. Soc.* **54**, 1145 (1932).
12. Lazier, W. A., U.S. Patent 2,079,414, 1937.
13. Schmidt, O., U.S. Patent 2,093,159, 1937.
14. Yan, T. Y., Albright, L. F., and Case, L. C., *Ind. Eng. Chem. Prod. Res. Dev.* **42**(2), 101 (1965).
15. Anello, L. G., Ridge, B., and Cunningham, W. J., U.S. Patent 3,356,747, 1967.
16. Case, L. C., and Yan, T. Y., U.S. Patent 3,314,987, 1967.
17. Evans, J. W., Casey, P. S., Wainwright, M. S., Trimm, D. L., and Cant, N. W., *Appl. Catal.* **7**, 31 (1983).
18. Evans, J. W., Cant, N. W., Trimm, D. L., and Wainwright, M. S., *Appl. Catal.* **6**, 355 (1983).
19. Stroupe, J. D., *J. Am. Chem. Soc.* **71**, 569 (1949).
20. Monti, D. M., Wainwright, M. S., and Trimm, D. L., *Ind. Eng. Chem. Prod. Res. Dev.* **24**, 397 (1985).
21. Monti, D. M., Cant, N. W., Trimm, D. L., and Wainwright, M. S., *J. Catal.* **100**, 17 (1986).
22. Monti, D. M., Cant, N. W., Trimm, D. L., and Wainwright, M. S., *J. Catal.* **100**, 28 (1986).
23. Brands, D. S., Poels, E. K., Krieger, T. A., Makarova, O. V., Weber, C., Veer, S., and Bliek, A., *Catal. Lett.* **36**, 175 (1996).
24. Brands, D. S., Poels, E. K., and Bliek, A., *in* "Proceedings, 11th International Congress on Catalysis, Baltimore (J. W. Hightower, W. N. Delgass, E. Iglesia, and A. T. Bell, Eds.), Vol. 101. p. 1085. Elsevier, Amsterdam; 1996.
25. Van de Scheur, F. T., van der Linden, B., Mittelmeijer-Hazeleger, M. C., Nazloomian, J. G., and Staal, L. H., *Appl. Catal. A* **111**, 63 (1994).
26. Van de Scheur, F. T., Brands, D. S., van der Linden, B., Luttikhuis, C. O., Poels, E. K., and Staal, L. H., *Appl. Catal. A* **116**, 237 (1994).
27. Van de Scheur, F. T., and Staal, L. H., *Appl. Catal. A* **108**, 63 (1994).
28. Van der Grift, C. J. G., Wielers, A. F. H., Joghi, B. P. J., van Beijnum, J., de Boer, M., Versluijs-Helder, M., and Geus, J. W., *J. Catal.* **131**, 178 (1991).
29. Kohler, M. A., Cant, N. W., Wainwright, M. S., and Trimm, D. L., *in* "Proceedings of the 9th International Congress on Catalysis, Calgary, 1988" (M. J. Phillips and M. Ternan, Eds.), p. 1043. Chem. Institute of Canada, Ottawa, 1988.
30. Agarwal, A. K., Cant, N. W., Wainwright, M. S., and Trimm, D. L., *J. Mol. Catal.* **43**, 79 (1987).
31. Agarwal, A. K., Wainwright, M. S., Trimm, D. L., and Cant, N. W., *J. Mol. Catal.* **45**, 247 (1988).
32. Evans, J. W., Wainwright, M. S., Cant, N. W., and Trimm, D. L., *J. Catal.* **88**, 203 (1984).
33. Kohler, M. A., Lee, J. C., Trimm, D. L., Cant, N. W., and Wainwright, M. S., *Appl. Catal.* **31**, 309 (1987).
34. Dell, R. M., Stone, F. S., and Tiley, P. F., *Trans. Faraday Soc.* **49**, 201 (1953).
35. Dell, R. M., Stone, F. S., and Tiley, P. F., *Trans. Faraday Soc.* **49**, 195 (1953).
36. Osinga, T. J., Linsen, B. G., and van Beek, W. P., *J. Catal.* **7**, 277 (1967).
37. Scholten, J. J. F., and Konvalinka, J. A., *Trans. Faraday Soc.* **65**, 2465 (1969).
38. Dvorák, B., and Pasek, J., *J. Catal.* **18**, 108 (1970).
39. Evans, J. W., Wainwright, M. S., Bridgewater, A. J., and Young, D. J., *Appl. Catal.* **7**, 75 (1983).
40. Cardona-Martínez, N., and Dumesic, J. A., *J. Catal.* **125**, 427 (1990).
41. Cardona-Martínez, N., and Dumesic, J. A., *Adv. Catal.* **38**, 149 (1992).
42. Becke, A. D., *J. Chem. Phys.* **98**, 5648 (1993).
43. Hehre, W. J., Radom, L., and Schleyer, P. v. R., "Ab Initio Molecular Orbital Theory," John Wiley & Sons, New York, 1986.
44. Davidson, E. R., *Int. J. Quantum Chem.* **69**, 241 (1998).
45. Hay, P. J., and Wadt, W. R., *J. Chem. Phys.* **82**, 270 (1985).
46. Hay, P. J., and Wadt, W. R., *J. Chem. Phys.* **82**, 299 (1985).
47. Wadt, W. R., and Hay, P. J., *J. Chem. Phys.* **82**, 284 (1985).
48. Kohn, W., Becke, A. D., and Parr, R. G., *J. Phys. Chem.* **100**, 12974 (1996).
49. Ziegler, T., *Chem. Rev.* **91**, 651 (1991).
50. Jaguar 3.5, S., Inc., Portland, Oregon, 1998.
51. Peng, C., and Schlegel, H. B., *Isr. J. Chem.* **33**, 449 (1993).
52. Natal Santiago, M. A., "Catalytic Reduction of Esters and Carboxylic Acids to Alcohols over Silica-Supported Copper." PhD thesis, University of Wisconsin, 1999.
53. Natal-Santiago, M. A., and Dumesic, J. A., *J. Catal.* **175**, 252 (1998).
54. Natal-Santiago, M. A., Hill, J. M., and Dumesic, J. A., *J. Mol. Catal.* **140**, 199 (1999).
55. Wachs, I. E., and Madix, R. J., *J. Catal.* **53**, 208 (1978).
56. Wachs, I. E., and Madix, R. J., *Appl. Surf. Sci.* **1**, 303 (1978).
57. Wachs, I. E., and Madix, R. J., *Surf. Sci.* **84**, 375 (1979).
58. Bowker, M., and Madix, R. J., *Surf. Sci.* **95**, 190 (1980).
59. Bowker, M., and J., M. R., *Surf. Sci.* **116**, 549 (1982).
60. Sexton, B. A., *Surf. Sci.* **88**, 299 (1979).
61. Sexton, B. A., Hughes, A. E., and Avery, N. R., *Surf. Sci.* **155**, 366 (1985).
62. Chesters, M. A., and McCash, E. M., *Spectrochimi. Acta A* **43**, 1625 (1987).
63. Camplin, J. P., and McCash, E. M., *Surf. Sci.* **360**, 229 (1996).
64. Russell, J. N., Gates, S. M., and Yates, J. T., *Surf. Sci.* **163**, 516 (1985).
65. Gellman, A. J., and Dai, Q., *J. Am. Chem. Soc.* **115**, 714 (1993).
66. Street, S. C., and Gellman, A. J., *J. Phys. Chem.* **100**, 8338 (1996).

67. Carlson, T. A., Agron, P. A., Thomas, T. M., and Grimm, F. A., *J. Elec. Spectrosc. Rel. Phenom.* **23**, 13 (1981).
68. Nyberg, G. L., and Anderson, S. E., *Surf. Sci.* **207**, 253 (1989).
69. Kojima, I., Sugihara, H., Miyazaki, E., and Yasumori, I., *J. Chem. Soc.: Faraday Trans. 1* **77**, 1315 (1981).
70. Harikumar, K. R., and Rao, C. N. R., *Catal. Lett.* **47**, 265 (1997).
71. Davies, P. R., and Mariotti, G. G., *J. Phys. Chem.* **100**, 19975 (1996).
72. Millar, G. J., Rochester, C. H., and Waugh, K. C., *J. Chem. Soc.: Faraday Trans.* **87**, 2795 (1991).
73. Lindner, T., Somers, J., Bradshaw, A. M., Kilcoyne, A. L. D., and Woodruff, D. P., *Surf. Sci.* **203**, 333 (1988).
74. Wiklund, M., Jaworowski, A., Strisland, F., Beutler, A., Sandell, A., Nyholm, R., Sorensen, S. L., and Andersen, J. N., *Surf. Sci.* **418**, 210 (1998).
75. Dai, Q., and Gellman, A. J., *J. Phys. Chem.* **97**, 10783 (1993).
76. Crapper, M. D., Woodruff, D. P., Bader, M., and Haase, J., *Surf. Sci.* **182**, L241 (1987).
77. Ryberg, R., *Chem. Phys. Lett.* **83**, 423 (1981).
78. Ryberg, R., *Phys. Rev. Lett.* **49**, 1579 (1982).
79. Ryberg, R., *Phys. Rev. B* **31**, 2545 (1985).
80. Prince, K. C., Holub-Krappe, E., Horn, K., and Woodruff, D. P., *Phys. Rev. B* **32**, 4249 (1985).
81. Holub-Krappe, E., Prince, K. C., Horn, K., and Woodruff, D. P., *Surf. Sci.* **173**, 176 (1986).
82. Bader, M., Puschmann, A., and Haase, J., *Phys. Rev. B* **33**, 7336 (1986).
83. Outka, D. A., Madix, R. J., and Stöh, J., *Surf. Sci.* **164**, 235 (1985).
84. Paul, J., and Rosén, A., *J. Catal.* **84**, 288 (1983).
85. Andersson, S., and Persson, M., *Phys. Rev. B* **24**, 3659 (1981).
86. Hofmann, P., Mariani, C., Horn, K., and Bradshaw, A. M., *Proc. Fourth Int. Conf. Solid Surf. Third Eur. Conf. Surf. Sci.* 541 (1980).
87. Stöh, J., Gland, J. L., Eberhardt, W., Outka, D., Madix, R. J., Sette, F., Koestner, R. J., and Doebler, U., *Phys. Rev. Lett.* **51**, 2414 (1983).
88. Wander, A., and Holland, B. W., *Surf. Sci.* **203**, L637 (1988).
89. Uvdal, P., and MacKerell, A. D., Jr., *Surf. Sci.* **393**, 141 (1997).
90. Madix, R. J., *Adv. Catal.* **29**, 1 (1980).
91. Yaws, C. L., "Chemical Properties Handbook." McGraw Hill Inc., New York, 1999.
92. Hammer, B., and Nørskov, J. K., *Nature* **376**, 238 (1995).
93. Stewart, W. E., and Caracotsios, M. C., "Athena Visual Workbench Version 4.0," Stewart & Associates Engineering Software, Inc., Madison, WI, 2000.
94. Watwe, R. M., Cortright, R. D., Nørskov, J. K., and Dumesic, J. A., *J. Phys. Chem. B* **104**, 2299 (2000).
95. De Donder, T., *in* "L'Affinité." Gauthier-Villers, Paris, 1927.
96. Boudart, M., *in* "Kinetics of Chemical Processes," Prentice-Hall, Englewood Cliffs, NJ, 1968.
97. Boudart, M., *in* "Physical Chemistry: An Advanced Treatise," (H. Eyring, Ed.), Vol. 7. Academic Press, San Diego, 1975.
98. Boudart, M., *J. Phys. Chem.* **87**, 2786 (1983).
99. Holstein, W. L., and Boudart, M., *J. Phys. Chem.* **101**, 9991 (1997).